

# **LEGIBILITY NOTICE**

A major purpose of the Technical Information Center is to provide the broadest dissemination possible of information contained in DOE's Research and Development Reports to business, industry, the academic community, and federal, state and local governments.

Although a small portion of this report is not reproducible, it is being made available to expedite the availability of information on the research discussed herein.

SEP 8 1989

Los Alamos National Laboratory is operated by the University of California for the United States Department of Energy under contract W-7405-ENG-4

LA-UR--89-2960

DE89 016777

TITLE HADRON DISTRIBUTIONS AT CERN - HEAVY ION EXPERIMENTS

AUTHOR(S) Barbara Jacak

SUBMITTED TO Proceedings, NATO Summer Institute on the Nuclear Equations of State, Peniscola, Spain, May 21 - June 3, 1989

#### DISCLAIMER

This report was prepared as an account of work sponsored by an agency of the United States Government. Neither the United States Government nor any agency thereof, nor any of their employees, makes any warranty, express or implied, or assumes any legal liability or responsibility for the accuracy, completeness, or usefulness of any information, apparatus, product, or process disclosed, or represents that its use would not infringe privately owned rights. Reference herein to any specific commercial product, process, or service by trade name, trademark, manufacturer, or otherwise does not necessarily constitute or imply its endorsement, recommendation, or favoring by the United States Government or any agency thereof. The views and opinions of authors expressed herein do not necessarily state or reflect those of the United States Government or any agency thereof.

By acceptance of this article the publisher recognizes that the U.S. Government retains a nonexclusive, royalty-free license to publish or reproduce the published form of this contribution or to allow others to do so for U.S. Government purposes.

The Los Alamos National Laboratory requests that the publisher identify this article as work performed under the auspices of the U.S. Department of Energy.

**Los Alamos** Los Alamos National Laboratory  
Los Alamos, New Mexico 87545

Form NO 535-96  
BY US MAIL 5-81

DISTRIBUTION

5 DOCUMENT IS UNLIMITED

# HADRON DISTRIBUTIONS AT CERN - HEAVY ION EXPERIMENTS

Barbara Jacak

Los Alamos National Laboratory  
Los Alamos, New Mexico 87545

HELIOS COLLABORATION

## I. INTRODUCTION

Ultrarelativistic heavy ion experiments have received considerable attention as they provide an opportunity to study large volumes of nuclear matter at high energy density. It has been predicted that such collisions can reach sufficiently high energy densities to deconfine the quarks and gluons,<sup>1</sup> forming a short-lived plasma.

The study of hadron distributions is an essential part of the search for new phenomena in heavy ion collisions. Hadron spectra have been measured over a large range of rapidities and transverse momenta for p-p collisions.<sup>2</sup> Comparison of the spectra from nucleus-nucleus collisions with those from p-p allows a search for effects beyond a simple superposition of nucleon-nucleon collisions. Pions are produced in the nucleon-nucleon collisions, and their rapidity distributions indicate the relevant center-of-mass in a nucleus-nucleus collision; these distributions are strongly affected by the multiple collisions undergone by the projectile nucleons. The hadron  $p_t$  spectra may indicate the degree of thermalization reached, or be modified by collective expansion of the highly excited central region.<sup>3,4,5,6</sup> Comparison of the  $p_t$  spectra of hadrons of different mass is necessary to sort out effects of collective expansion and thermal emission.

Thermal models<sup>7,8</sup> predict that strange particle production should be greatly enhanced if a plasma is formed in the reaction. However, the final hadronization process is very complicated and may obscure signals from the plasma.<sup>9</sup> Also, it has not been established that thermal equilibrium is achieved in ultrarelativistic heavy ion collisions, and the strangeness production predicted for a plasma or for a chemically equilibrated hadron gas is quite different than that predicted by non-equilibrium models.<sup>10</sup> As these collisions do not result in a baryon-free central region, effects of secondary collisions on the strange particle abundances may also be important.<sup>11</sup> Clearly, there is an urgent need for experimental data; HELIOS measures strangeness production via the kaons.

A great deal of information is provided by the  $p_t$  and rapidity distributions of protons in heavy ion collisions. The proton rapidity distributions indicate the degree of stopping in the collision, and the rapidity dependence of the  $p_t$  spectra can provide some clues about the stopping mechanism. It is not currently known whether collisions of the projectile nucleons beyond the first are best described as collisions of "wounded" nucleons or as collisions of normal, but slower, protons and neutrons. Effects of rescattering in the spectator matter are also likely to be important and should strongly influence the proton distributions.

## II. EXPERIMENTAL

The results presented in this paper are taken from the HELIOS experiment at the CERN SPS. HELIOS (High Energy Lepton and Ion Spectrometer) measures the energy flow over the whole solid angle with good resolution in energy and angle, to select events with large amounts of energy deposited. The experiment measures the influence of this large energy deposit on charged particle multiplicity flow, hadron  $p_t$  distributions, lepton pairs and photons. Data have been collected for 60 GeV/A O and 200 GeV/A p, O, and S beams on various targets.

The overall charged particle multiplicity is measured via two highly segmented silicon pad counters placed several centimeters behind the target. Each pad is read out into a discriminator for trigger information, and into an ADC to allow resolution of multiple hits.

Single particles are detected in HELIOS using a magnetic spectrometer examining the events through a narrow azimuthal gap in the calorimeter coverage. This slit covers the pseudorapidity interval 1.0-1.9. To support the calorimeter, the slit is filled with aluminum hexcell, 0.03 radiation lengths thick. The slit opening is 10 cm vertically, so the azimuthal coverage varies from 2.1% at  $\eta=1.9$  to 0.75% at  $\eta=1.0$ . A magnet with a momentum kick of 80 MeV/c and two high resolution drift chambers provide the momentum measurement. The horizontal coordinate is measured via the drift time ( $\sigma_x \sim 200\mu\text{m}$ ) and the vertical coordinate via charge division ( $\sigma_y \sim 1.0\text{cm}$ ). Particle identification is provided by two time-of-flight scintillator hodoscopes behind the second drift chamber, with a flight path from the target of 5 meters. The first wall covers the small angle section of the acceptance, and has a time resolution  $\sigma_t \sim 250$  ps. The second wall has about half the resolution. Its timing is adequate to resolve pions and protons at large angles, and it provides redundancy in the forward part of the spectrometer.

## III. CHARGED PARTICLE PSEUDORAPIDITY DISTRIBUTION

The pseudorapidity distribution of charged particles from 60 and 200 GeV/A O beams colliding with several targets<sup>12</sup> is shown in Fig. 1. For each target, three multiplicity distributions are shown, corresponding to cuts on the tail, knee and plateau of the transverse energy distribution measured in the calorimeters. These cuts sample different regions of impact parameter: the plateau region comes from collisions without full overlap of projectile and target, full overlap occurs just before the knee in the  $E_t$  spectrum, and the tail corresponds to very central collisions, with fluctuations to high  $E_t$ .

The peak of the distributions  $dN_{ch}/d\eta$  is clearly shifted towards smaller pseudorapidities with increasing  $E_t$  and increasing target mass. This reflects the displacement of the effective center of mass due to the increasing number of participating target nucleons. The backward displacement is accompanied by a slight reduction of the width of the pseudorapidity distributions, which is expected as the degree of stopping increases. Note that the observed widths are considerably larger than those expected from the isotropic decay of a fireball. The maximum rapidity density is independent of beam energy and target mass, and is a function of  $E_t$  only.

The solid curves in Fig. 1 are absolute predictions from the IRIS 3.05 generator,<sup>13</sup> which is based on the dual parton model.<sup>14</sup> The IRIS prediction does not fully reproduce the backward rapidity shift with increasing  $E_t$ . This is a possible indication of the importance of target fragmentation and intranuclear cascading, neither of which is included in the model. Additionally, IRIS may underestimate the stopping of the projectile by the target nucleus.

## IV. PION TRANSVERSE MOMENTUM DISTRIBUTIONS

Figure 2 shows the transverse momentum spectra  $d\sigma/dp_t^2$  for negative particles, dominantly pions, measured in the external spectrometer.<sup>15</sup> The spectra are corrected

by Monte Carlo for effects of detector acceptance and resolution, particle decay, and conversion of photons in the material upstream of the spectrometer. The three spectra correspond to p+W, O+W and S+W collisions. The spectra are for central collisions, and reflect different thresholds on  $E_t$  measured in the calorimeters, corresponding to approximately 25% of the geometrical cross section. It is clear that the  $p_t$  spectra cannot be described by a single exponential. Fitting an exponential distribution to limited  $p_t$  ranges in the S+W data yields inverse slopes of 210 MeV/c for  $0.5 < p_t < 1.5$  GeV/c, and 85 MeV/c for  $0.075 < p_t < 0.25$  GeV/c.

The rise in cross section at low  $p_t$  has been reported at more central rapidities in heavy ion collisions at CERN,<sup>16</sup> in p-nucleus collisions at Fermilab,<sup>17</sup> and in cosmic ray data.<sup>18</sup> In our data, which extends into the target rapidity region, 40% of the pions observed arise from the low  $p_t$  excess. Consequently, a process which creates 2-4 soft pions per p+W central collision is required. The effect is somewhat smaller at higher rapidities.<sup>16</sup>

The rapidity dependence may help distinguish among possible soft pion production mechanisms. Pions produced by rescattering in the target or from the decays of  $\Delta$  and  $N^*$  resonances should be observed close to the target rapidity, in contrast to a central rapidity source undergoing a collective expansion, such as proposed in reference 18.

In Fig. 2, the  $p_t$  spectrum from p+W is compared to a parameterization of minimum bias p-p data (given by the full line). In addition to the low  $p_t$  excess, enhanced production of particles at high  $p_t$  is evident. This was first observed by Cronin, et al.<sup>19</sup> The spectra of nucleus-nucleus collisions closely resemble those from p-nucleus collisions, and a similar enhancement at high  $p_t$  occurs.

Figure 3 compares the shapes of the  $p_t$  spectra from different projectiles by plotting ratios of the spectra as a function of  $p_t$ . The ratios are normalized to unity in the range  $0.25 < p_t < 0.5$  GeV/c, since the absolute ratio is not meaningful for data taken with different  $E_t$  thresholds. A clear projectile dependence is observed. Both  $\sigma_{SW}/\sigma_{PW}$  and  $\sigma_{OW}/\sigma_{PW}$  deviate from unity. A larger projectile results in a larger high  $p_t$  enhancement.

It has been suggested that the Cronin effect is due to rescattering of partons<sup>20</sup> or pions in the target nucleus. This must lead to a larger enhancement of high  $p_t$  particles at target rapidities compared to central rapidities.

The projectile dependence is also visible in the mean transverse momentum, when the values of  $\langle p_t \rangle$  are determined in the range 0.4 to 2.0 GeV/c.  $\langle p_t \rangle$  is calculated in the given range, then extrapolated to the mean of the entire spectrum under the assumption of a purely exponential shape. The requirement  $p_t > 400$  MeV/c excludes the low  $p_t$  rise, so the result may be compared with p-p collisions. It is important to note that the  $\langle p_t \rangle$  values obtained can be affected by deviations in the spectral shape from exponential. We find  $\langle p_t \rangle = 413 \pm 5$ ,  $408 \pm 10$  and  $372 \pm 10$  MeV/c for S+W, O+W and p+W respectively, each with a systematic error of 10 MeV/c.  $\langle p_t \rangle$  varies with rapidity due to kinematics in p+p and p+A collisions. In our S+W data,  $\langle p_t \rangle$  decreases by  $30 \pm 10$  MeV/c from  $1.45 < y < 1.9$  to  $0.9 < y < 1.45$ . Within errors, this kinematic effect does not change the projectile dependence of the  $p_t$  distribution.

To study the  $E_t$  dependence of the negative particle  $p_t$  spectra, data for S+W and S+Pt collisions are combined as they show no difference (within statistical accuracy). Figure 4 shows  $\langle p_t \rangle$  as a function of  $E_t$ .  $\langle p_t \rangle$  rises by 50 MeV/c from peripheral collisions to those with  $\sim$  half-overlap of the target and projectile. It then remains approximately constant to very central collisions in which the highest energy densities are achieved.

In peripheral collisions the number of participants varies strongly with impact parameter. According to the Cronin effect,  $\langle p_t \rangle$  increases with the number of

participants. This rise is 20 MeV/c in p-nucleus collisions<sup>19</sup>, and larger in nucleus-nucleus collisions. Once full overlap of target and projectile are reached, the Cronin effect should not increase further with  $E_t$ . However,  $\langle p_t \rangle$  in the sulfur data becomes constant before full overlap is reached.

The constancy of  $\langle p_t \rangle$  with  $E_t$  can be interpreted with either a hydrodynamic or microscopic picture of nucleus-nucleus collisions. Hydrodynamic models have the option of including a hadron-parton phase transition or a pure hadron phase. In case of a phase transition, a constant  $\langle p_t \rangle$  arises from the coexistence stage of the two phases in a natural way, due to the constant temperature and pressure, i.e., the absence of strong hydrodynamical expansion effects at energy densities not too much above the critical density.<sup>5,24</sup> For a purely hadronic system a constant  $\langle p_t \rangle$  can be obtained if the hadrons always decouple at the same number density (at the same temperature independent of the initial state) and if there is only longitudinal hydrodynamic expansion. Numerical calculations for a pure hadron phase do, however, show transverse expansion effects,<sup>5</sup> resulting in a  $\langle p_t \rangle$  rise of about 30% over the energy density range accessible in this experiment. Microscopic models can give approximately constant  $\langle p_t \rangle$  since the hadronization process masks the increased  $\langle p_t \rangle$  of the partons with increasing number of parton interactions leading to higher  $E_t$ .

## V. KAON PRODUCTION

Particles in the external spectrometer are identified by calculating the mass from the momentum determined by the drift chambers and the flight time measured in the scintillator walls. Electrons with  $p_t < 175$  MeV/c are removed via a momentum-dependent cut in  $\text{mass}^2$ .  $\text{Mass}^2$  is a better variable than mass because the resolution broadens the peaks, which can extend below 0. At higher values of  $p_t$  the electron contamination is negligible. The  $\text{mass}^2$  spectra in Fig. 5 show clear peaks for pions, kaons and protons. These spectra are fit with the sum of three gaussians centered at the  $\text{mass}^2$  of the  $\pi$ , K and p; the areas of the gaussians yield the numbers of the different types of particles. Simultaneous fitting of all three peaks allows determination of the particle distributions into the momentum region where the peaks begin to overlap. The contribution of the tails of the other peaks is correctly subtracted in this procedure. As the flight time is measured twice, the  $\text{mass}^2$  spectra are very clean and no background subtraction is necessary. The spectrometer acceptance, K and  $\pi$  decay, and multiple scattering in the spectrometer material are simulated by Monte Carlo and the data corrected for these effects.

Figure 6 shows the  $p_t$  spectra of  $K^+$  and  $K^-$  for  $y = 1.0-1.3$ . The  $K^+$   $p_t$  spectrum is flatter than  $K^-$ , in contrast to p-p collisions, where they have approximately the same slope. For S+W, the  $K^-$  inverse slope is between 300 and 350 MeV/c; in p-p collisions the inverse slope for kaons is 350 MeV/c. It is important to note that the different slopes for  $K^+$  and  $K^-$  imply a different behavior of the  $K/\pi$  ratios in S+W than in p-p collisions.

A convenient way to compare the spectra of K and  $\pi$  is to plot the invariant cross sections as a function of the transverse mass, where  $M_t = \sqrt{p_t^2 + m^2}$ . In p-p collisions the data show an approximate scaling behavior with  $M_t$ , i.e., the  $M_t$  spectra for different particles fall roughly onto the same curve. Though emission of particles from a thermal source would give rise to  $M_t$  scaling, the reason for this scaling in p-p collisions is unclear. Also it is important to note that the scaling is only approximate; there are deviations of factors of 3-4 in cross section between the curves for different particles. The slopes for different particle  $M_t$  spectra are rather similar, however. Figure 7 shows  $M_t$  spectra of  $K^+$ ,  $K^-$  and  $\pi^-$  from S+W. The points corresponding to the different particles do fall roughly onto one curve, but the  $K^+$  spectrum is somewhat flatter than  $K^-$  and  $\pi^-$ . This deviation implies a rising ratio  $K^+/\pi^+$  for increasing  $p_t$ .

Figure 8 shows the ratios of charged kaons to pions as a function of  $p_t$  in the rapidity range 1.0-1.3. The upper points represent  $K^+/\pi^+$  and the lower points  $K^-/\pi^-$ .

The dashed and solid lines show the  $K/\pi$  ratios observed in p-p collisions at the ISR for  $\sqrt{s} = 23 \text{ GeV}^{21,22}$  for positive and negative particles, respectively. In order to compare with nucleus-nucleus data at rapidity 1.0-1.3, the p-p results have been scaled down from the ratios observed at midrapidity. As the external spectrometer measures  $K/\pi$  about 1 unit below the peak in the rapidity distribution of the energy and particle flow in S+W, the ratios for p-p collisions are also scaled from midrapidity by 1 unit. We scale from the effective center of mass rapidity determined by the energy/particle flow peak because each projectile nucleon collides with several target nucleons in S+W reactions. Thus the projectile nucleons undergo an energy degradation during the reaction, so the average  $\sqrt{s}$  is lower than the  $\sqrt{s}$  of the first collision. In p-p data all collisions occur at the same  $\sqrt{s}$ . It is important to scale by the distance from midrapidity rather than the distance from the target fragmentation region because kaons are produced predominantly in the central region. The ranges showed by the solid and dashed lines in Fig. 8 reflect the uncertainties in the scaling procedure.

Comparison with expectations from p-p collisions allows a search for excess strange particle production in nucleus-nucleus collisions. It is clear from Fig. 8 that at low  $p_t$  there is no excess of strange particles in S+W. The  $K/\pi$  ratios are perhaps somewhat lower than those observed in p-p collisions, as one might expect from the rise in cross section for very low  $p_t$  pions. For  $p_t > 400 \text{ MeV}/c$ , the  $K^+/\pi^+$  ratio observed in S+W begins to exceed that in p-p collisions.  $K^-/\pi^-$  does not show an excess in the  $p_t$  range accessible. The increasing excess of  $K/\pi$  with  $p_t$  has been observed in 14.5 GeV/A Si + Au collisions by E802 at the AGS.<sup>23</sup> Though their data are concentrated at high  $p_t$ , there is a small region of overlap between the  $p_t$  coverage of HELIOS and E802. In this region, the  $K/\pi$  ratios for both positive and negative particles are very similar even though the bombarding energies differ by more than an order of magnitude. We find no strong  $E_t$  dependence of the rise in  $K/\pi$  above values from p-p collisions.

Such an increase in  $K/\pi$  has been predicted by Mattiello and coworkers, using the Relativistic Quantum Molecular Dynamics model of the nucleon and produced particle transport in heavy ion collisions.<sup>11</sup> The calculation produces a final kaon yield approximately double that of the primary nucleon-nucleon collisions, with the additional kaons arising from rescattering of the produced particles and participating nucleons in the surrounding target matter. The kaons produced by rescattering have the correct  $p_t$  dependence: they are produced with a larger  $\langle p_t \rangle$  than kaons from the initial collisions. The magnitude of the rescattering effect must depend strongly on the baryon density, and comparison of predicted rescattering effects with results from HELIOS where  $p/\pi^+$  is approximately 10-20% and with results from E802 where  $p/\pi^+$  approaches 100% should determine whether this explanation of the excess  $K/\pi$  is correct.

## VI. CONCLUSIONS

We have presented  $dN/d\eta$  distributions for charged particles from nucleus-nucleus collisions at the CERN SPS. We have also studied the transverse momentum distributions of pions and kaons in the external spectrometer, in the vicinity of  $y = 1$ .

Negative particle spectra, consisting mainly of pions, show an excess at high  $p_t$  in p-nucleus and nucleus-nucleus collisions, compared to p-p. This is known as the Cronin effect, and is more pronounced for larger projectiles. The Cronin effect probably arises from parton or hadron rescattering. There is a large excess of soft pions in p-nucleus and nucleus-nucleus collisions. The process yielding these pions is not currently understood, the low  $p_t$  excess is larger at target-like rapidities than at midrapidity. The  $\pi^-/\pi^+$  rises from very peripheral to more central collisions, but then remains constant with further increases in  $E_t$ . This is not consistent with expectations for a thermalized hadron gas, unless it undergoes longitudinal expansion only. It is not clear how to interpret the constant  $\pi^-/\pi^+$ , but it must be stressed that the isolation of transverse expansion effects from the *shape* of the  $p_t$  spectra alone remains questionable as long as the observed excess at low  $p_t$  and the Cronin effect at high  $p_t$  are not simultaneously accounted for.

We observe an excess in  $K/\pi$  over results from p-p collisions for positive particles. This excess causes the  $K^+ p_t$  spectrum to be flatter than the  $K^-$  spectrum, which has a slope comparable to  $K^-$  in p-p data. A similar effect at comparable values of  $p_t$  are observed in lower energy collisions at the AGS. The kaon enhancement is consistent with expectations from rescattering of pions and kaons formed in the primary nucleon-nucleon collisions. The interpretation of these results will be aided by comparison with results from p-nucleus collisions, currently being analyzed.

## REFERENCES

1. See, for example, Proceedings of the Quark Matter Conferences in Brookhaven (1984), Helsinki (1984) and Asilomar (1986).
2. A review of these results may be found in: Giacomelli and M. Jacob, Phys. Rep., 55B, 1 (1979).
3. K. Redlich and H. Satz, Phys. Rev., D33, 3747 (1986).
4. K.S. Lee and U. Heinz, Univ. Regensburg, preprint TPR-88-16 (1988).
5. M. Kataja, P.V. Ruuskanen, L. McLerran and H. von Gersdorff, Phys. Rev., D34, 2755 (1986).
6. X. Wang and R. Hwa, Phys. Rev., D35, 3409 (1987).
7. J. Rafelski and B. Mueller, Phys. Rev. Lett., 48, 1066 (1982).
8. P. Koch, B. Mueller, and J. Rafelski, Phys. Rep., 142, 167 (1986).
9. K.S. Lee, M.J. Rhodes-Brown and U. Heinz, Phys. Rev., C37, 1452 (1986).
10. B. Friman, Proceedings of Quark Matter '88, Lenox, Mass., to be published in Nucl. Phys.
11. R. Mattiello, H. Sorge, H. Stoecker and W. Greiner, Univ. of Frankfurt, preprint UFTP 233/1989.
12. T. Akesson, *et al.*, (HELIOS collaboration), submitted to Nucl. Phys. B, June 1989.
13. J.P. Pansart, Saclay, preprint DPhPE 89-04, March 1989, and references within.
14. A. Capella and J. Tran Thanh Van, Phys. Lett., 93B, 146 (1980).
15. T. Akesson, *et al.*, (HELIOS collaboration), submitted to Z. Phys. C, July 1989.
16. H. Stroebele, *et al.*, (NA35 collaboration), Z. Phys., C38, (1988).
17. D.A. Garbutt, *et al.*, Phys. Lett., 67B, 355 (1977).
18. T.W. Atwater, P.S. Freier and J.L. Kapusta, Phys. Lett., 199B, 30 (1987).
19. J.W. Cronin, *et al.*, Phys. Rev., D11, 3105 (1975).
20. D. Antreasyan, *et al.*, Phys. Rev., D19, 764 (1979).



20. M. Lev and B. Petersson, Z. Phys., C21, 155 (1983).
21. B. Alper, *et al.*, Nucl. Phys., B100, 237 (1975).
22. K. Guettler, *et al.*, Nucl. Phys., B116, 77 (1976).
23. P. Vincent, *et al.*, (E802 collaboration), Proceedings of Quark Matter '88, Lenox, Mass., to be published in Nucl. Phys.
- P. Vincent, *et al.*, (E802 collaboration), Z. Phys., C38, 38 (1988).
24. E. V. Shuryak, Z. Phys., C38, 165 (1988).

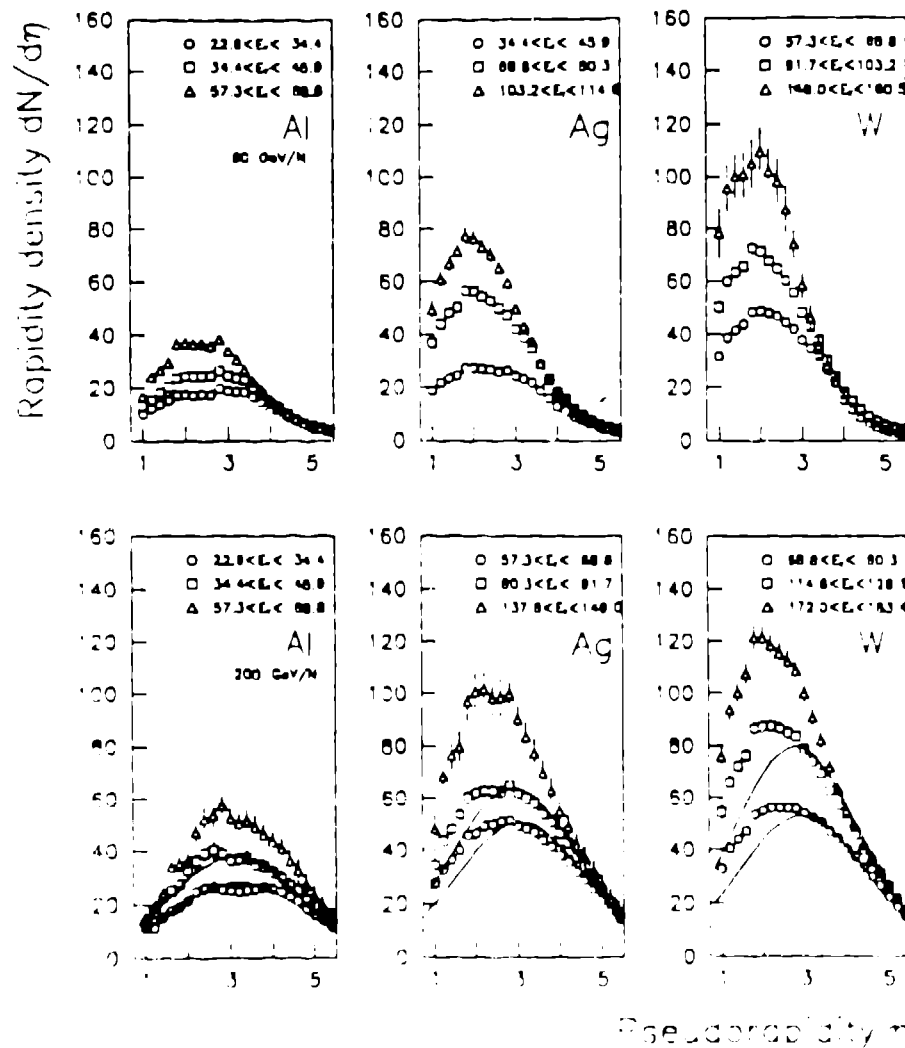


**Fig. 1.** Distribution of pseudorapidity density for three selected windows in  $E$  within the trigger region ( $-0.1 < \eta < 2.9$ ). a) 60 GeV A-O; b) 200 GeV A-O. The errors shown are statistical only. The lines indicate IRIS predictions.

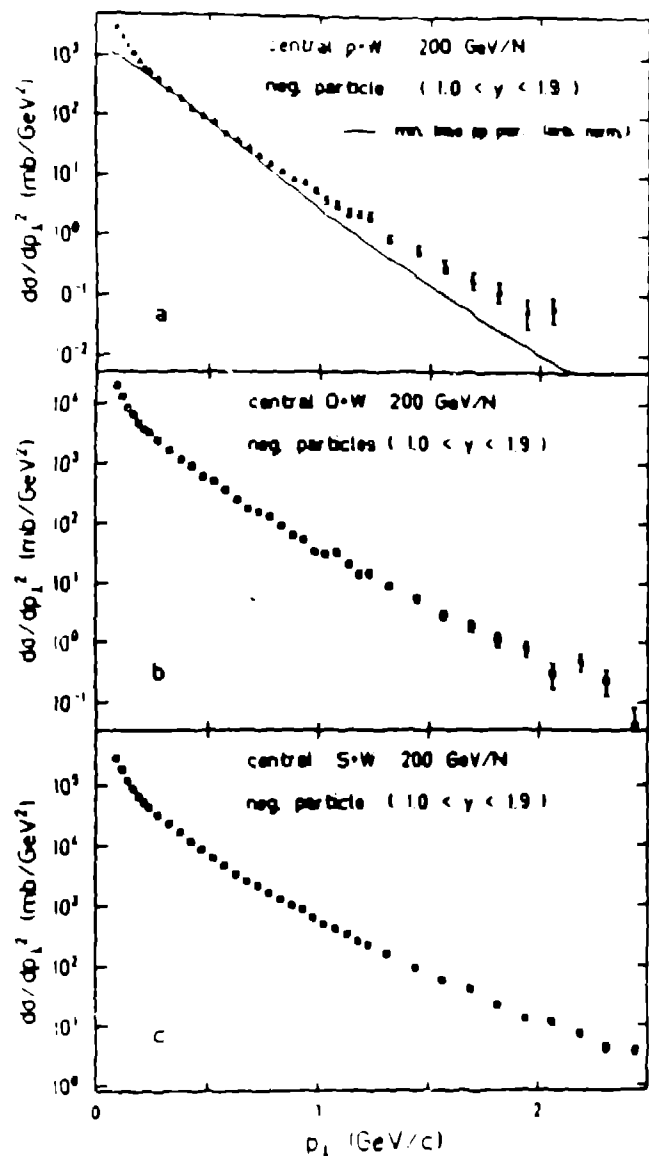
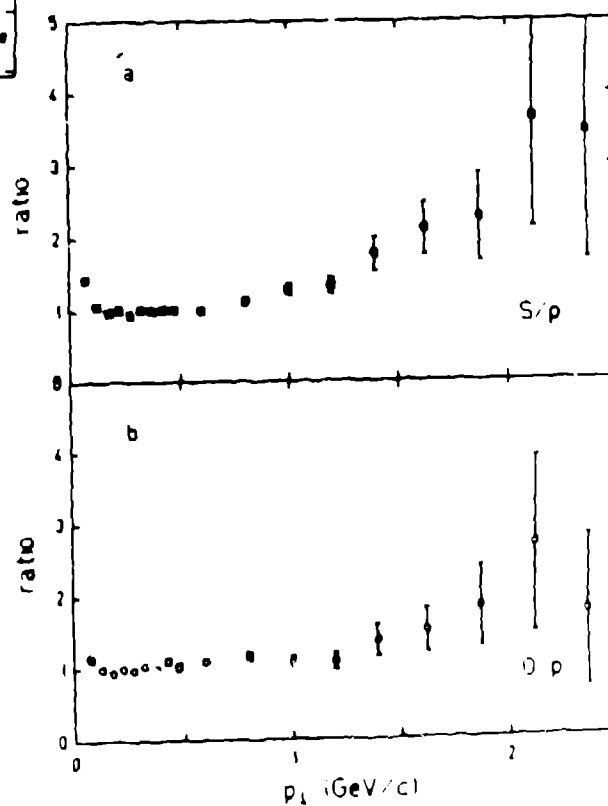


Fig. 2.  $1/p_t dN/dp_t$  for central collisions of 200 GeV/A p, O and S beams with a W target. Central collisions are selected by a cut in  $E_t$ ,  $E_t > 10, 60$ , and 80 GeV, respectively. The solid line shows a parameterization of p-p data.

Fig. 3. Ratios of the spectra shown in Fig. 2. Since different  $E_t$  thresholds are used, the ratios are normalized to unity.



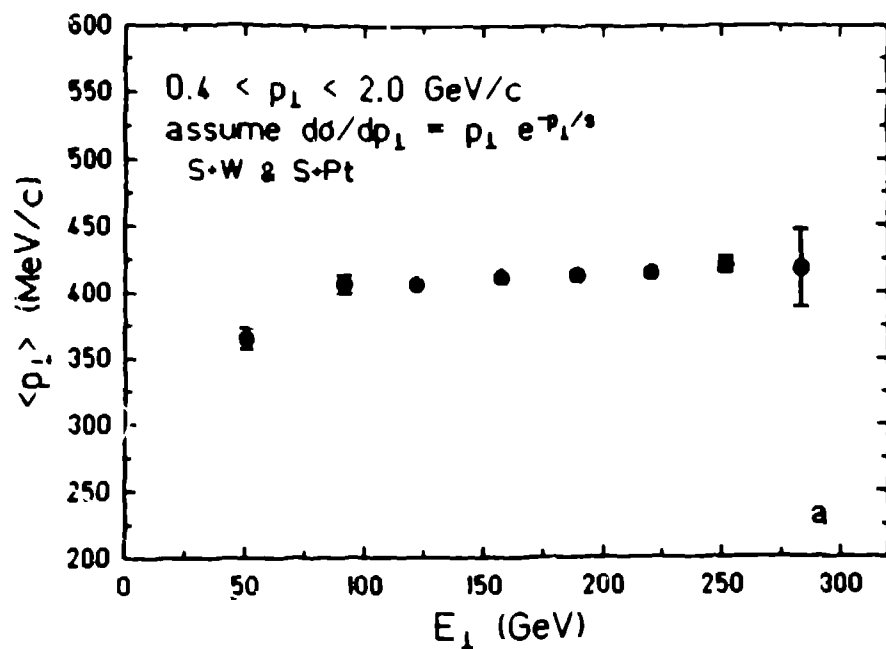


Fig. 4.  $\langle p_t \rangle$  as a function of  $E_t$  measured in the region  $-0.1 < \eta < 2.9$ , for the combined data set S+W and S+Pt. The mean determined in the range  $0.4 < p_t < 2.0 \text{ GeV/c}$  is converted to  $\langle p_t \rangle$  for the full range assuming an exponential spectrum.

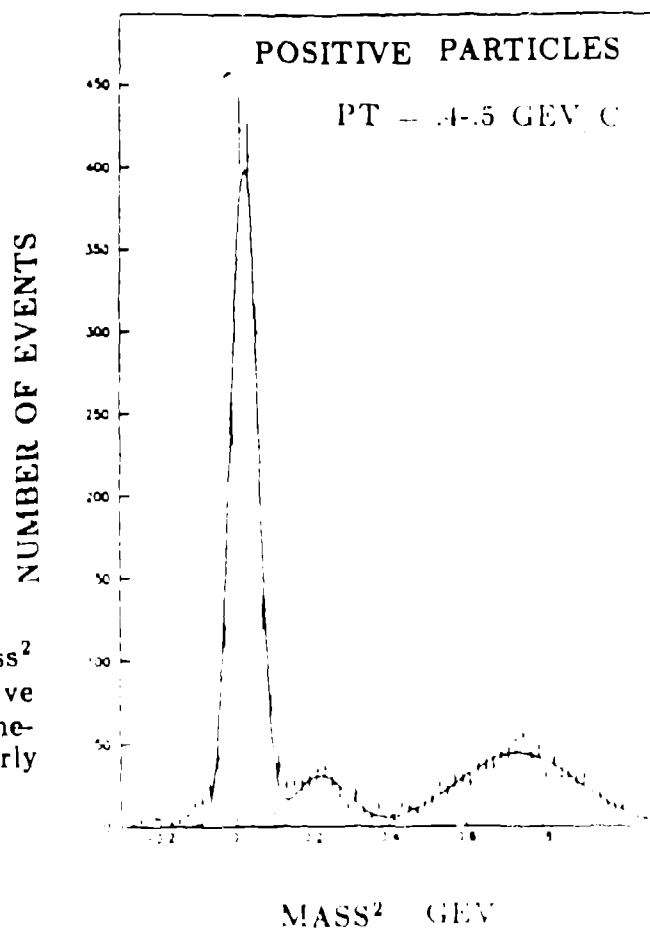


Fig. 5. An example of the mass<sup>2</sup> spectrum (in GeV/c<sup>2</sup>) for positive particles in the external spectrometer. The  $\pi$ , K and protons are clearly visible.

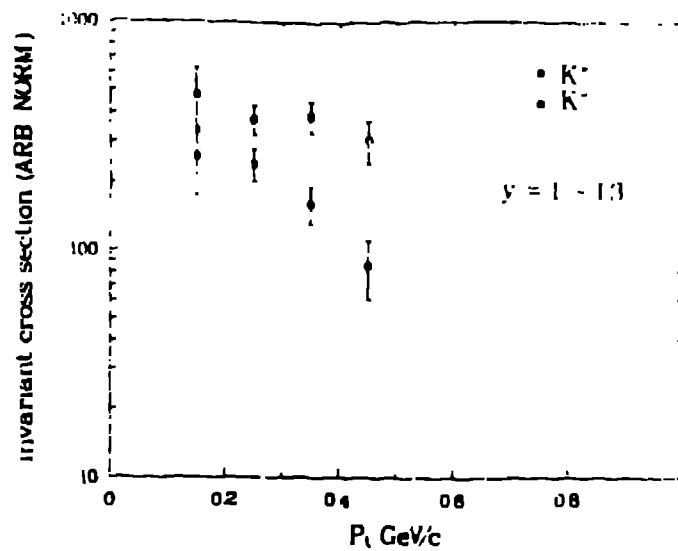


Fig. 6.  $1/p_t dN/dp_t$  for  $K^+$  and  $K^-$  produced in S+W collisions, in the rapidity region  $1.0 < y < 1.3$ . No  $E_t$  selection has been made in these data.

Fig. 7. Invariant cross sections for  $K^+$ ,  $K^-$ , and  $\pi^-$  from S+W collisions, as a function of  $M_t$ .

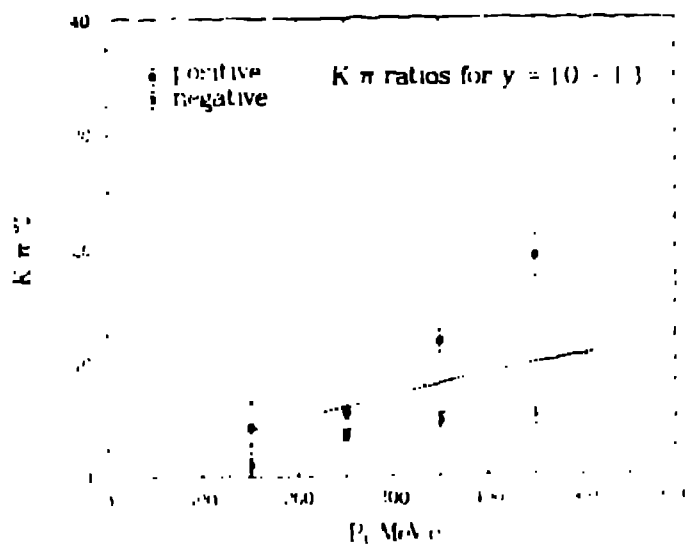
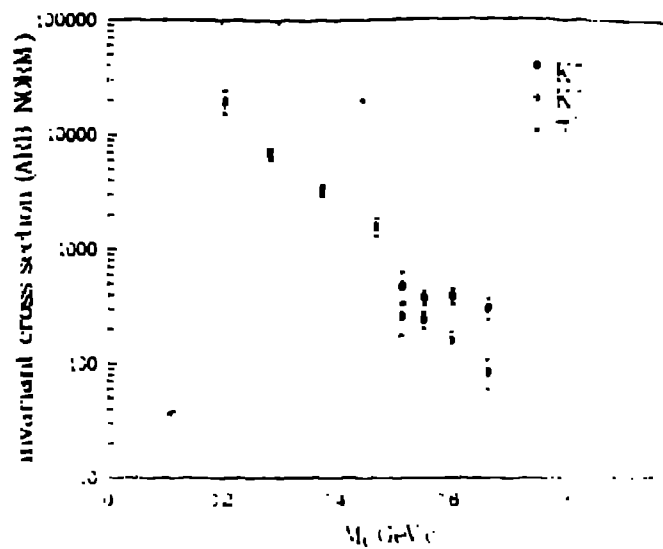


Fig. 8.  $K/\pi$  ratios vs.  $p_t$  for S+W collisions. The lines represent results from p-p collisions, scaled by 1 unit of rapidity down from midrapidity to match the spectrometer acceptance for S+W.